
A simple blind-denoising filter inspired by electrically coupled photoreceptors in the retina

Yang Yue
Peking University
yueyang999@pku.edu.cn

Liuyuan He
Peking University
liyhe@pku.edu.cn

Gan He
Peking University
hegan@pku.edu.cn

Jian.K.Liu
University of Leicester
jian.liu@leicester.ac.uk

Kai Du*
Department of Neuroscience
Karolinska Institutet
Kai.Du@ki.se

Yonghong Tian*
Peking University
yhtian@pku.edu.cn

Tiejun Huang
Peking University
tjhuang@pku.edu.cn

Abstract

Photoreceptors in the retina are coupled by electrical synapses called “gap junctions”. It has long been established that gap junctions increase the signal-to-noise ratio of photoreceptors. Inspired by electrically coupled photoreceptors, we introduced a simple filter, the PR-filter, with only one variable. On BSD68 dataset, PR-filter showed outstanding performance in SSIM during blind denoising tasks. It also significantly improved the performance of state-of-the-art convolutional neural network blind denoising on non-Gaussian noise. The performance of keeping more details might be attributed to small receptive field of the photoreceptors.

1 Introduction

Photoreceptors are the first stage of our early visual system, which transfer lights signals impinged on the retina into electrical signals^{1,2}. The photoreceptors produce large amount of noises during phototransduction process³. Through millions of years of evolution, our retina has developed a simple strategy for denoising—making photoreceptors electrically coupled via synapses called “gap junctions”^{4,5,6,7,8}. It was proposed that photoreceptor electrical couplings are able to increase signal-to-noise ratio and important for noise filtering^{4,5,9}. However, the denoising mechanism for large-scale, electrically coupled photoreceptor network remains unexplored. Importantly, the strategy of making our biologic “photo-sensors” electrically coupled is entirely different from electronic photo-sensors in cameras or other devices, which must be strictly isolated from each other.

Here, we explored the denoising effects in the photoreceptor network with gap junctions. The aims of this study are multiple: (1) to gain insights into denoising mechanisms of electrical coupled photoreceptors in the retina; (2) to apply the biology-derived principle into machine denoising.

The structure of this paper is organized as follows: First, we applied the “spike-triggered average (STA)” method^{10,11,12} to estimate the receptive field of individual photoreceptors in a biologically detailed photoreceptors network. The STA analysis indicate single photoreceptor has a small receptive field (Fig.2C), suggesting single photoreceptor summarize information very locally. Next, we constructed a photoreceptor-filter (PR-filter) – a grid network with electrically coupled PRs. We extensively tested the PR-filter on various types of noise. The SSIM performance of the PR-filter

exceeds any other classic spatial filters. At last, we combined the PR-filter with deep convolutional neural network (CNN). Our results indicates that the PR-filter can significantly improve the performance of the state-of-the-art CNN denoising on blind non-Gaussian noise¹³, not only increasing the signal-to-noise ratio but also keeping more details in vision.

Over all, our work is the first to apply the gap junctions in the machine denoising tasks and the first to show the gap junctions can be directly integrated in the modern AI architecture, which is significant for understanding evolution emergence of electrical couplings between photoreceptors and may inspire blind denoising in machine learning.

2 Background

2.1 Photoreceptor noise

Photoreceptors noises mainly originate from two parts¹⁴: (1) dark noise produced by intracellular activities, (2) ambient illuminations. In low-light intensity conditions, the noise can be several log units higher than signals^{3,15}.

2.2 Gap junctions in the retina

Gap junctions are electrical synapses which allow cells to directly communicate with electrical signals⁵. Retina has a layer-wised structure, while photoreceptors (rods and cones) are located in the first layer (Fig.1). Gap junctions are abundant in each layers of the retinal (Fig.1), suggesting the gap junction is fundamental to retina signal processing¹⁶.

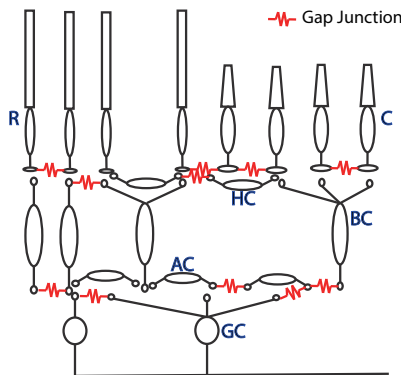


Figure 1: Gap junctions in the retina circuitry. Information of light stimulus flow through three layers of neurons: cone (C) and rod (R) as photoreceptors, cone and rod bipolar cells (BC), ganglion cells (GC).

2.3 Receptive field and STA analysis

In neuroscience, “receptive field” refers to a specific region of stimuli (in space) that can affect a neuron’s response¹⁷. The STA analysis is one of the most popular methods which has been widely used in studying receptive field in visual and auditory system¹⁰². The STA was initially designed for spiking neurons, but it can also apply to non-spiking neurons, such as BC¹⁸. For estimating non-linear receptive field, one should refer to other methods such as spike-triggered covariance (STC)¹⁹ and Bayesian method²⁰.

To compute the STA, the whole stimulus time is divided into k bins equally. Let x_i denotes the stimulus vector preceding i th bin and here the mean of stimuli are assumed to be zero. And y_i denotes

the spike number in i_{th} bin. The STA is given by

$$STA = \frac{1}{n_s} \sum_{i=1}^{n_s} y_i x_i \quad (1)$$

where n_s is the total number of spikes. The STA method requires stimulus to be strictly ‘‘spherically symmetric’’, such as white noise^{21,22}. If the stimulus distribution is not spherically symmetric, ZCA whitening can be applied before computing STA.

3 Experiments

3.1 STA analysis of electrically coupled photoreceptors

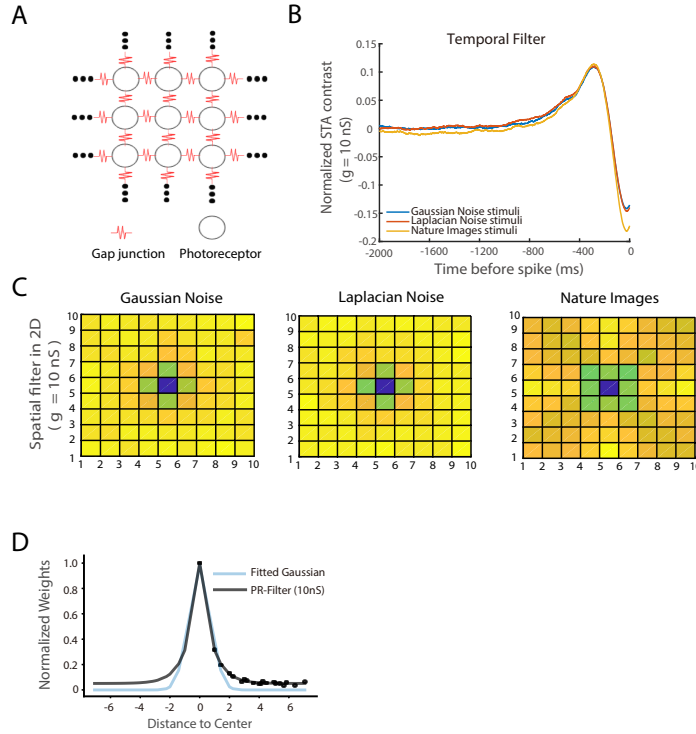


Figure 2: (A) Schematic diagram for 10x10 Photoreceptor network. Photoreceptors are organized as grid and gap junctions connect them as edges. (B) Normalized weights in temporal filters. The negative peaks appear at ~ 24 ms prior to the spikelet, indicating stimulus perturbation at this time point, on average, make maximal negative correlation to the spikelet. (C) STA spatial filters(receptive fields) under different stimuli for the center cell in network. White Gaussian Noise is labeled as ‘Gaussian Noise’. Laplacian noise and nature images are whitened before fed into model. When corresponding line in (B) reaches its minimum value, we computed STAs for all photoreceptors in the network and ‘‘froze’’ them at ~ 24 ms prior to the spikelet, which reveal the spatial receptive field for the centered neuron in the network. (D) PR filter compares with Gaussian filter.

To gain insights into the functional role of gap junctions at the network level, we investigated the spatiotemporal receptive field of photoreceptors in a network, wherein gap junction couplings are the only connections among cells. We constructed a biologically detailed model for the photoreceptor, including phototransduction cascade and ion channels (Appendix Fig.A1.1, Table.A1.1, Table.A1.2, and Table.A1.3). The model is described as follows:

$$C_m \frac{dv_m}{dt} = \sum g_{ion}(v_m - e_{ion}) + g_{leak}(v_m - e_{leak}) + I_{gap} + I_{photo} \quad (2)$$

$$I_{gap} = g_{gap}(v_m - v_{gap}) \quad (3)$$

where v_m is the membrane voltage of photoreceptor, C_m is the membrane voltage capacitance, v_{gap} is the voltage of gap junction, I_{gap} and I_{photo} are currents from gap junction and phototransduction respectively, e_{ion} and e_{leak} are the voltage potentials of ion channel and leak, g_{leak} is leak conductance, and g_{ion} is ion channel conductance in Hodgkin-Huxley form²³. The photoreceptor model can generate photocurrents in close match to available electrophysiology data (Appendix Fig.A1.2)²⁴. The topology of the network is grid-like (10×10 in size) and consisted of 100 photoreceptors (Fig.2A). In such a network, a neuron can only form connections to neighboring neurons and there is no long-range connections²⁵. All simulations were performed in the NEURON simulator²⁶.

To first investigate receptive field of photoreceptors under different stimuli, we feed the network with three types of inputs: Gaussian noise, Laplacian noise and natural images. Fig.2B shows the temporal STAs computed at the center neuron of the network. For all tested stimuli, our results show “off-center” receptive field of the center neuron, suggesting gap junctions provide inhibition-like effects at this moment (Fig.2C). Interestingly, the shapes of the spatial receptive field are similar to a narrow Gaussian filter($\sigma=0.7358$)(Fig.2D), but with a heavier "tail", suggesting that the receptive field of single photoreceptor is largely weighted on the local connections, but sum up more information from larger area compared to a narrow Gaussian filter.

3.2 PR-filter on blind-denoising

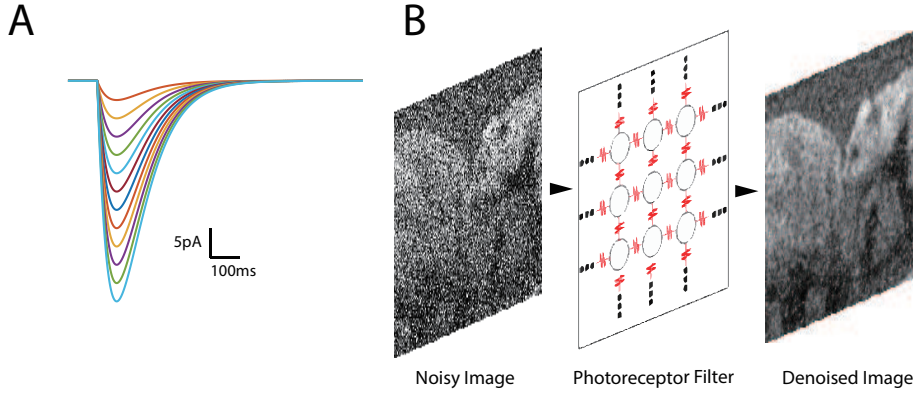


Figure 3: (A) Simplified photocurrent curves in the PR-filter. (B) Value of pixels in input image is converted into stimuli for network model and the peak values of the voltage responses is normalized as the output image.

The STA analysis indicate the electrically coupled photoreceptor network can form self-organized receptive field, similar to a narrow Gaussian filter. We wonder if the photoreceptor network can be directly applied for image denoising. However, one problem in applying the biologically detailed network on high resolution images is the computation cost, due to simulated phototransduction cascade (Appendix Fig.A1). To this end, we simplified the network in the following procedure: (1) We removed all ion channels and only kept passive leak channels. The model was reduced to:

$$C_m \frac{dv_m}{dt} = g_{leak}(v_m - e_{leak}) + I_{gap} + I_{photo}^* \quad (4)$$

(2) We used simplified photocurrents to replace the phototransduction cascade model. The photocurrents were reduced to double-exponential function:

$$I_{photo}^* = I_{dark} - g_{max} \frac{\tau_2(e^{-\frac{t}{\tau_1}} - e^{-\frac{t}{\tau_2}})}{(\tau_1 - \tau_2) \frac{\tau_2}{\tau_1} \frac{\tau_1}{\tau_1 - \tau_2}} \quad (5)$$

¹Red mark stands for best performance of this line.

²Intensity dependent Gaussian noise.

³Blind noise mixed by five regular noise types, which are white Gaussian, intensity dependent Gaussian(I.D.G.), Laplacian, Salt&Pepper, and uniform.

⁴Blind noise mentioned above, but excluded two kinds of Gaussian noise.

Table 1: All PSNR comparison of single filter

Noise Type	noisy	Adaptive Median	Average	Gaussian	Max	Mean	Median	Min	PR
Gaussian	9.3931	12.3257	16.4323	16.7648	5.6420	16.8155	14.7134	7.4840	<i>19.4910</i>
	12.0365	14.9079	19.1847	19.6653	7.6740	19.6792	18.1044	8.9699	<i>20.9816</i>
	14.9113	17.6838	21.5659	22.2076	10.2093	22.1672	20.9178	10.9068	<i>21.7804</i>
	18.1941	20.7064	23.6390	24.6108	12.9497	24.3491	23.4640	13.2402	<i>23.3808</i>
I.D.G.	9.3962	12.3250	16.4365	16.7691	5.6442	16.8200	14.7149	7.4880	<i>19.5363</i>
	11.6292	14.5065	18.8063	19.2645	7.3250	19.2853	17.6505	8.7198	<i>20.6644</i>
	14.9198	17.6923	21.5705	22.2112	10.2112	22.1714	20.9270	10.9191	<i>21.7553</i>
	17.7218	20.2876	23.3770	24.2926	12.5780	24.0730	23.1347	12.9066	<i>23.1438</i>
Laplacian	9.5985	13.2473	16.6411	16.9802	5.5888	17.0283	15.8758	7.4579	<i>19.4907</i>
	12.0132	15.7000	19.1456	19.6166	7.2323	19.6343	19.3830	8.7341	<i>20.8815</i>
	14.4932	18.2277	21.2598	21.8724	9.2729	21.8447	21.9666	10.3296	<i>21.7843</i>
	17.8840	21.4520	23.4909	24.4264	12.1308	24.1948	24.4911	12.6902	<i>23.2115</i>
Salt&Pepper	9.6453	28.3222	16.5263	16.8384	5.2340	16.8919	19.8959	7.3248	<i>18.9588</i>
	12.0806	30.7300	19.0877	19.5262	6.4557	19.5544	25.8218	8.5177	<i>20.2686</i>
	15.0880	32.2882	21.6591	22.2638	8.4892	22.2465	28.2621	10.4893	<i>21.2754</i>
	18.0933	32.8780	23.6104	24.5444	10.7724	24.3107	28.8849	12.6374	<i>22.8880</i>
Uniform	8.8903	11.1816	15.8579	16.1635	5.6221	16.2197	13.1821	7.4633	<i>19.1190</i>
	11.7585	13.7830	18.9400	19.4126	8.1607	19.4283	16.5059	9.1614	<i>20.8624</i>
	14.3920	16.2600	21.1588	21.7747	10.5340	21.7410	19.0915	11.0152	<i>21.6886</i>
	17.6805	19.3204	23.3418	24.2517	13.2001	24.0344	21.9098	13.3752	<i>23.0765</i>
Blind	9.5785	13.9324	16.3319	16.6370	5.4844	16.6862	16.1899	7.4002	<i>19.4510</i>
	12.4169	17.3056	19.3707	19.8453	7.2606	19.8553	20.2933	8.8709	<i>21.0081</i>
	15.2791	20.3255	21.7421	22.3774	9.4325	22.3364	23.0744	10.8026	<i>21.7454</i>
Blind NG	9.6814	14.2938	16.7078	17.0474	5.5096	17.0955	16.7126	7.4115	<i>19.5333</i>
	14.1590	19.0992	20.9855	21.5724	8.5531	21.5534	22.5579	9.9460	<i>21.4669</i>
	17.7802	28.5549	23.4309	24.3325	10.6422	24.1224	27.7345	12.4137	<i>21.5955</i>

Table 2: All SSIM comparison of single filter

Noise Type	noisy	Adaptive Median	Average	Gaussian	Max	Mean	Median	Min	PR
Gaussian	0.0660	0.0883	0.1731	0.2083	0.1598	0.2053	0.1479	0.0219	<i>0.3969</i>
	0.1204	0.1561	0.2668	0.3176	0.1820	0.3115	0.2458	0.0623	<i>0.5023</i>
	0.1950	0.2437	0.3703	0.4360	0.2388	0.4249	0.3544	0.1308	<i>0.5695</i>
	0.3005	0.3608	0.4860	0.5640	0.3256	0.5462	0.4789	0.2329	<i>0.6299</i>
I.D.G.	0.0660	0.0882	0.1730	0.2083	0.1597	0.2053	0.1477	0.0220	<i>0.3976</i>
	0.1113	0.1449	0.2526	0.3011	0.1763	0.2956	0.2309	0.0546	<i>0.4884</i>
	0.1954	0.2443	0.3708	0.4365	0.2391	0.4255	0.3547	0.1314	<i>0.5694</i>
	0.2841	0.3432	0.4698	0.5466	0.3126	0.5298	0.4614	0.2172	<i>0.6215</i>
Laplacian	0.0702	0.1150	0.1795	0.2158	0.1447	0.2127	0.1816	0.0219	<i>0.4040</i>
	0.1217	0.1869	0.2653	0.3162	0.1538	0.3098	0.2976	0.0537	<i>0.4993</i>
	0.1870	0.2733	0.3566	0.4206	0.1882	0.4099	0.4112	0.1012	<i>0.5614</i>
	0.2955	0.4038	0.4778	0.5554	0.2601	0.5378	0.5482	0.1864	<i>0.6248</i>
Salt&Pepper	0.0737	0.8839	0.1805	0.2167	0.0775	0.2135	0.5545	0.0284	<i>0.3980</i>
	0.1364	0.9237	0.2720	0.3241	0.0800	0.3161	0.7846	0.0596	<i>0.4936</i>
	0.2518	0.9374	0.3930	0.4624	0.1196	0.4462	0.8313	0.1233	<i>0.5638</i>
	0.4180	0.9397	0.5148	0.5972	0.2093	0.5711	0.8409	0.2291	<i>0.6225</i>
Uniform	0.0566	0.0568	0.1558	0.1879	0.1841	0.1853	0.1122	0.0220	<i>0.3725</i>
	0.1127	0.1165	0.2575	0.3067	0.2472	0.3013	0.1938	0.0826	<i>0.4958</i>
	0.1778	0.1859	0.3507	0.4138	0.3254	0.4039	0.2776	0.1719	<i>0.5601</i>
	0.2796	0.2932	0.4675	0.5440	0.4255	0.5275	0.3944	0.3043	<i>0.6215</i>
Blind	0.0681	0.1377	0.1737	0.2088	0.1293	0.2058	0.1870	0.0263	<i>0.3900</i>
	0.1341	0.2387	0.2790	0.3324	0.1422	0.3247	0.3300	0.0633	<i>0.4640</i>
	0.2215	0.3513	0.3878	0.4563	0.1878	0.4425	0.4624	0.1306	<i>0.5621</i>
Blind NG	0.0722	0.1461	0.1826	0.2193	0.1321	0.2161	0.2087	0.0221	<i>0.4061</i>
	0.1838	0.3089	0.3460	0.4090	0.1620	0.3980	0.4400	0.0919	<i>0.5300</i>
	0.3715	0.7518	0.4989	0.5797	0.2091	0.5558	0.7612	0.2065	<i>0.6192</i>

where $I_{dark} = 40pA$, $\tau_{1} = 64ms$, $\tau_{2} = 68ms$, and g_{max} controls the amplitude of I_{photo}^* . We found the choice of kinetic parameters for the wave-form is not critical, as long as there is a certain time course. (3) The network is still grid-like as in previous detailed network, but the size of the network can be expanded in accordance with image resolutions, wherein each photoreceptor encodes single pixel.

Thus, we constructed a photoreceptor based filter, the PR-filter, with only one tunable parameter—the gap junction strength. In addition, no inference or prior knowledge of noise is required. Therefore, it can be applied for blind denoising. Next, we tested the PR-filter on the Berkeley segmentation dataset(BSD68)^{27,13} dataset and compared our results with classic spatial filters. In addition to a variety of regular noise types, we also generated two types of “blind-noise”. We listed both peak *signal-to-noise ratio* (PSNR) and *structural similarity index* (SSIM) of the denoised images. Surprisingly, we found the PR-filter dominates the SSIM performance on nearly all noise types (both high level and low level, Table 2, see Appendix 2 for parameter details), suggesting the PR-filter denoising aims to remain more details of the original images. The only exception to the PR-filter is the Salt&Pepper noise. Even if to this particular noise type, the PR-filter achieves relative good performance in both PSNR and SSIM. As to the PSNR index, the PR-filter achieves highest performance on nearly all types of noises in case the noise levels are high, while it still remains good performance in case the noise levels are low (Table 1). In comparison, all other classic filters have weak performance when dealing with either regular or blind noise types (Table 1). Overall, the PR-filter shows superior performance in SSIM index and excellent performance in PSNR index.

3.3 PR-filter improves CNN blind denoising on non-Gaussian noise

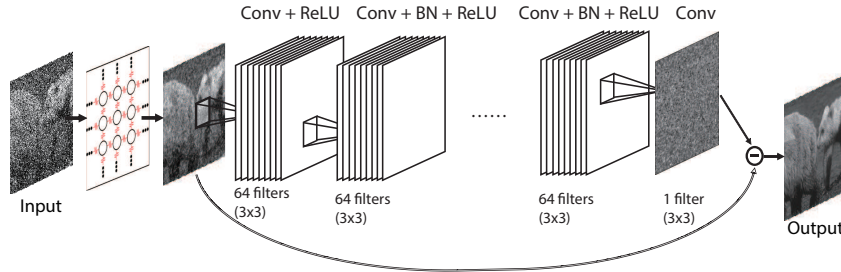


Figure 4: Architecture for PR filter + DnCNN. Noisy images are filtered by PR filter first before used as training data for DnCNN. We use 400 images of size 180×180 for training²⁸. $128 \times 3,000$ patches of size 50×50 are cropped from the 400 images to train our model. For testing we use 68 natural images from BSD68. The weights are initialized by the method in²⁹. We train our network using Adam optimizer with a initial learning rate of 0.001. Our network is trained for 50 epochs with a mini-batch size of 128. The learning rate is divided by 10 upon reaching 30 epochs.

Table 3: blind denoising result of Network

Type	noisy	DnCNN	G-filter+CNN	PR-filter+CNN
PSNR	9.5785	24.1443	22.7434	23.5233
	12.4169	26.1321	25.1654	25.5654
	15.2791	27.8843	27.1413	27.4664
SSIM	0.0681	0.7624	0.7124	0.7305
	0.1341	0.8265	0.7953	0.8065
	0.2215	0.8729	0.8547	0.8628

Table 4: blind non-Gaussian denoising result of Network

Type	noisy	DnCNN	G-filter+CNN	<i>PR-filter+CNN</i>
PSNR	9.6814	21.93	23.07	<i>23.56</i>
	14.1590	24.4234	26.3956	<i>26.5412</i>
	17.7802	31.4521	32.7721	<i>33.5383</i>
SSIM	0.0722	0.6884	0.7197	<i>0.7414</i>
	0.1838	0.7762	0.8307	<i>0.8406</i>
	0.3715	0.9357	0.9526	<i>0.9594</i>

Most of the existing CNN blind denoising methods are essentially Gaussian denoising³⁰, which limits their general applications on non-Gaussian noise in reality. We wonder if combining the PR-filter with CNN denoising would improve the performance of the CNN blind denoising on non-Gaussian noise. We selected the framework “DnCNN”¹³, which is the state-of-the-art CNN blind denoising method, and re-implemented the DnCNN in Tensorflow²⁹. The blind noises were identical to those in the section 3.2. The idea is to first process the raw noisy image by the PR-filter, then trained the DnCNN with the filtered image data (“PR-filter+DnCNN”, Fig.4). This architecture is similar to our visual system: noisy signals are first processed in the retina, and then sent to visual cortex for further improvements on details.

Our results indicates the PR-filter+DnCNN outperforms original DnCNN by ~ 2 dB in PSNR and 0.02-0.07 in SSIM while performing blind denoising on blind non-Gaussian noises (Table 4). Although the Gaussian filter can also improve the performance of DnCNN, it is less effective than the PR-filter (Table 4). Fig.5 illustrates the visual effects of the blind denoising on blind non-Gaussian noise. As to blind noises including Gaussian noise, DnCNN performs slightly better than PR-filter+DnCNN (~ 0.5 dB in PSNR and 0.01-0.02 in SSIM, Table 3), suggesting the PR-filter doesn’t significantly weaken the ability of CNN blind denoising on noises including Gaussian.

Why the PR-filter can improve the performance of DnCNN on non-Gaussian blind noise? To gain insights into its working mechanism, we next analyzed the noise distributions before/after the PR-filter. Intriguingly, we found the PR-filter can regularize the noise distributions: In most cases we encountered, the filtered image noise was squeezed towards the center and formed distributions similar to Gaussian (Fig 6D-E, also see examples in Fig 6A and 6B). In very few cases where the original noise distributions appear discontinuous, the filtered image noise was still squeezed towards the center but formed distributions similar to mixture of Gaussian (Fig. 6C). The DnCNN adopted a strategy called “residual learning”, which aims to learn the distribution of the noise. As the DnCNN was initially optimized for Gaussian¹³, by changing irregular noise distributions closer to Gaussian, the PR-filter is able to improve the performance of DnCNN on non-Gaussian noise.

4 Discussions

In this study, inspired by the electrically coupled photoreceptors, we constructed a photoreceptor-filter (PR-filter). Although this simple filter contains only one variable, it exhibits excellent performance in blind denoising. In particular, it outperforms all classic spatial filters in SSIM index (with the only exception when dealing with Salt&Pepper noise). In addition, it also significantly improves the performance (in both PSNR and SSIM) of the state-of-the-art CNN blind denoising on non-Gaussian noise. Why the PR-filter can keep good details of the image while efficiently removing noise? One plausible explanation is the receptive field revealed by STA analysis, which is similar to a narrow Gaussian filter. The photoreceptor in the PR-filter mostly sums up information from a very small patch, thus, it is more sensitive to details such as edges and lines. Why the PR-filter negatively impacts the performance of DnCNN on blind Gaussian noise? The reasons might be: (1) we haven’t done extensive parameter search for the gap junction value. (2) the original noise distribution of blind Gaussian noise is already close to Gaussian. Can PR-filter also improve the performance of BM3D³¹? BM3D is essentially a non-blind denoiser and requires estimation of “noise level” (σ). Its performance might be more sensitive to the estimated noise level, rather than distribution of noise itself. As we expected, the PR-filter greatly improve the performance of BM3D given $\sigma=25$, but slightly negatively impact BM3D given $\sigma=50$ (Appendix Table A3.1).

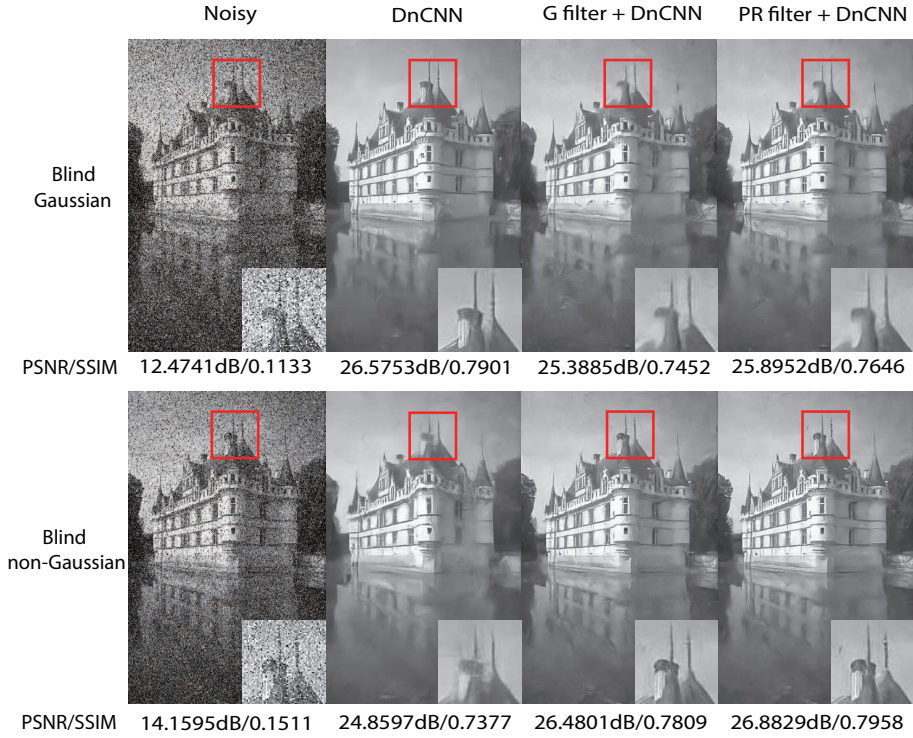


Figure 5: Example image for filter + DnCNN. Conductance for gap junctions in PR filter is 10nS and σ for G filter is 2.

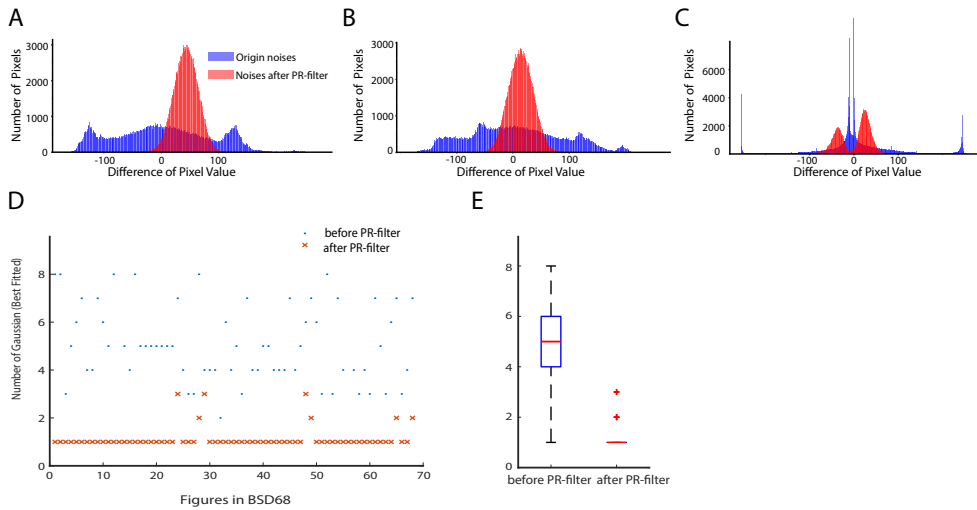


Figure 6: Noise distributions before and after the PR-filter. (A-C) Example noise distributions. (D) Fitting noise distributions before and after the PR-filter with Gaussian functions. (E) Statistics of fitted Gaussian numbers. Note most of the noise distribution after the PR-filter can be fitted by single Gaussian.

Appendix1

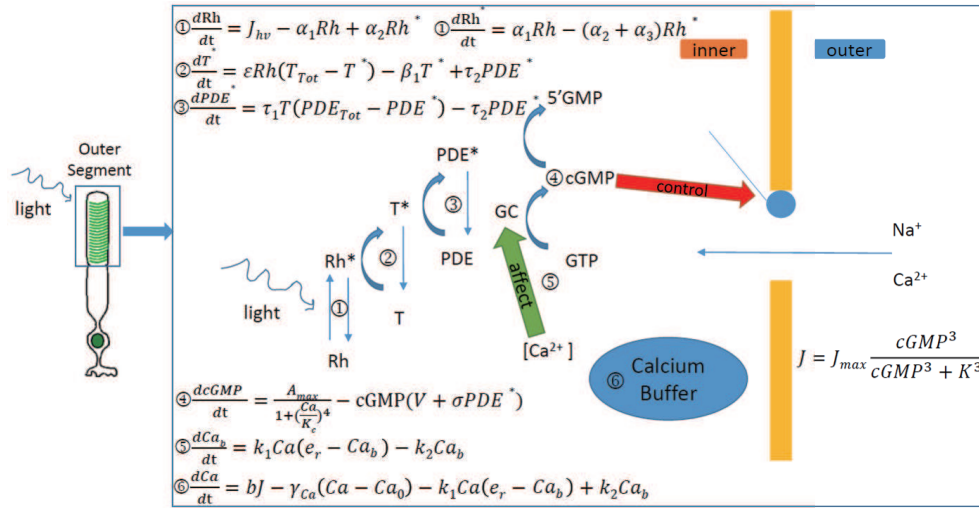


Figure A1.1: The mechanism of phototransduction

The phototransduction cascade model was adapted from^{32,33,34} and we retuned the parameters in the NEURON simulator. The model framework is illustrated in Figure A1.1 and parameters are listed in Table A1.1, Table A1.2 and Table A1.3.

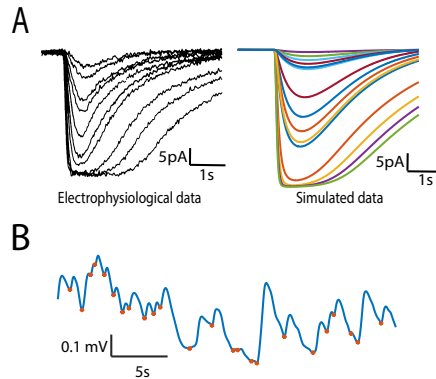


Figure A1.2: Photoreceptor network model for STA analysis. (A) Photocurrents in physiological data (left, adapted from²⁴) and our detailed model (right). (B) Sample voltage response trace under white Gaussian noise. Red marker donates the peak point (viewed as ‘spike’) in trace.

For modeling the whole rod photoreceptor, we add different ion mechanisms^{34,35,36,37,38} in rod soma, which are listed in Table A1.3.

Table A1.1: The parameter of phototransduction mechanism

Parameter	Value
α_1	0.05 ms^{-1}
α_2	$0.0000003 \text{ ms}^{-1}$
α_3	0.00003 ms^{-1}
ε	$0.0005 \text{ uM}^{-1} \text{ ms}^{-1}$
T_{Tot}	1000 uM
β	$0.00025 \text{ uMms}^{-1} \text{ pA}^{-1}$
τ_1	$0.0002 \text{ uM}^{-1} \text{ ms}^{-1}$
τ_2	0.005 ms^{-1}
PDE_{Tot}	100 uM
σ	$0.001 \text{ uM}^{-1} \text{ ms}^{-1}$
A_{max}	0.0656 uMms^{-1}
K_c	0.1 uM
V	0.0004 ms^{-1}
k_1	$0.0002 \text{ uM}^{-1} \text{ ms}^{-1}$
k_2	0.0008 ms^{-1}
e_r	500 uM
b	$0.00025 \text{ uMms}^{-1} \text{ pA}^{-1}$
γ_{Ca}	0.05 ms^{-1}
C_{a0}	0.1 uM
J_{max}	5040 pA
K	10 uM

Table A1.2: The initial parameter of phototransduction differential equation

Initial parameter	Value
Ca_0	0.3 uM
Ca_{b0}	34.9 uM
$cGMP_0^*$	2 uMms^{-1}

Table A1.3: The ion mechanism of photoreceptor

Mechanism	Conductance Value
Calcium channel	2 mS/cm^2
Ca-dependent potassium channel	0.5 mS/cm^2
Delayed rectifying potassium channel	2.0 mS/cm^2
Noninactivating potassium channel	0.85 mS/cm^2
Nonselective cation channel channel	3.5 mS/cm^2
Leak	0.6 mS/cm^2
Calcium Buffer	Not applicable

Appendix2

For testing the performance of PR-filter, we used five common noises, including white Gaussian, intensity dependent Gaussian, Laplacian, Salt&Pepper, and uniform, and we mixed these noises pixelwisely and generated two kinds of blind noises.

For blind noise including Gaussian noise, we generated blind noises by adding noises pixelwisely in the sequence of Gaussian, intensity dependent Gaussian, Laplacian, Salt&Pepper, and uniform, where we selected parameters randomly, but we made the average PSNR of noisy images to be ~ 9 , ~ 12 , and ~ 15 respectively.

For blind noise excluding Gaussian noise, we made the average PSNR of noisy images to be ~ 9 , ~ 14 , and ~ 18 respectively.

Appendix3

Table A3.1: Denoising result of BM3D

Type	blind Gaussian	blind non-Gaussian	blind Gaussian $\sigma_{BM3D}=25$		blind non-Gaussian		blind Gaussian $\sigma_{BM3D}=50$		blind non-Gaussian	
			BM3D	PR+BM3D	BM3D	PR+BM3D	BM3D	PR+BM3D	BM3D	PR+BM3D
PSNR	9.5785	9.6814	10.3207	19.7015	10.4458	19.7273	15.2713	19.7419	15.6448	19.7933
	12.4169	14.1590	13.9610	21.6104	16.7682	23.2251	22.7856	22.7088	24.4656	24.1791
	15.2791	17.7802	19.1426	23.9680	22.9378	25.3970	24.7373	24.5023	25.5649	25.3711
SSIM	0.0681	0.0722	0.0758	0.4623	0.0805	0.4740	0.1519	0.4761	0.1625	0.4853
	0.1341	0.1838	0.1653	0.5400	0.2618	0.5825	0.5723	0.5999	0.6518	0.6454
	0.2215	0.3715	0.3706	0.6274	0.5811	0.6957	0.6561	0.6650	0.6702	0.6752

References

1. Richard H Masland. The neuronal organization of the retina. *Neuron*, 76(2):266–280, 2012.
2. Jonathan B Demb and Joshua H Singer. Functional circuitry of the retina. *Annual review of vision science*, 1:263–289, 2015.
3. Foster Rieke and Denis A Baylor. Single-photon detection by rod cells of the retina. *Reviews of Modern Physics*, 70(3):1027, 1998.
4. Steven H DeVries, Xiaofeng Qi, Robert Smith, Walter Makous, and Peter Sterling. Electrical coupling between mammalian cones. *Current Biology*, 12(22):1900–1907, 2002.
5. W Howard Evans and Patricia EM Martin. Gap junctions: structure and function. *Molecular membrane biology*, 19(2):121–136, 2002.
6. Sabrina Asteriti, Claudia Gargini, and Lorenzo Cangiano. Mouse rods signal through gap junctions with cones. *Elife*, 3:e01386, 2014.
7. Sabrina Asteriti, Sten Grillner, and Lorenzo Cangiano. A cambrian origin for vertebrate rods. *Elife*, 4:e07166, 2015.
8. Sabrina Asteriti and Lorenzo Cangiano. Slow light response kinetics in rods points towards a perturbation of the normal cellular milieu. *The Journal of physiology*, 593(13):2975–2976, 2015.
9. Peter H Li, Jan Verweij, James H Long, and Julie L Schnapf. Gap-junctional coupling of mammalian rod photoreceptors and its effect on visual detection. *Journal of Neuroscience*, 32(10):3552–3562, 2012.
10. EJ Chichilnisky. A simple white noise analysis of neuronal light responses. *Network: Computation in Neural Systems*, 12(2):199–213, 2001.
11. Tatyana O Sharpee. Computational identification of receptive fields. *Annual review of neuroscience*, 36:103–120, 2013.

12. Jon Touryan, Gidon Felsen, and Yang Dan. Spatial structure of complex cell receptive fields measured with natural images. *Neuron*, 45(5):781–791, 2005.
13. Kai Zhang, Wangmeng Zuo, Yunjin Chen, Deyu Meng, and Lei Zhang. Beyond a gaussian denoiser: Residual learning of deep cnn for image denoising. *IEEE Transactions on Image Processing*, 26(7):3142–3155, 2017.
14. Fred Rieke and Denis A Baylor. Origin and functional impact of dark noise in retinal cones. *Neuron*, 26(1):181–186, 2000.
15. Robert B Barlow, Robert R Birge, Ehud Kaplan, and Jack R Tallent. On the molecular origin of photoreceptor noise. *Nature*, 366(6450):64, 1993.
16. Stewart A Bloomfield and Béla Völgyi. The diverse functional roles and regulation of neuronal gap junctions in the retina. *Nature Reviews Neuroscience*, 10(7):495, 2009.
17. Frédéric E Theunissen, Stephen V David, Nandini C Singh, Anne Hsu, William E Vinje, and Jack L Gallant. Estimating spatio-temporal receptive fields of auditory and visual neurons from their responses to natural stimuli. *Network: Computation in Neural Systems*, 12(3):289–316, 2001.
18. Jian K Liu, Helene M Schreyer, Arno Onken, Fernando Rozenblit, Mohammad H Khani, Vidhyasankar Krishnamoorthy, Stefano Panzeri, and Tim Gollisch. Inference of neuronal functional circuitry with spike-triggered non-negative matrix factorization. *Nature communications*, 8(1):149, 2017.
19. Liam Paninski. Convergence properties of some spike-triggered analysis techniques. In *Advances in neural information processing systems*, pages 189–196, 2003.
20. Il Memming Park and Jonathan W Pillow. Bayesian spike-triggered covariance analysis. In *Advances in neural information processing systems*, pages 1692–1700, 2011.
21. Tatyana Sharpee, Nicole C Rust, and William Bialek. Analyzing neural responses to natural signals: maximally informative dimensions. *Neural computation*, 16(2):223–250, 2004.
22. Julian Jakob Bussgang. Crosscorrelation functions of amplitude-distorted gaussian signals. 1952.
23. Alan L Hodgkin and Andrew F Huxley. A quantitative description of membrane current and its application to conduction and excitation in nerve. *The Journal of physiology*, 117(4):500–544, 1952.
24. DA Baylor and BJ Nunn. Electrical properties of the light-sensitive conductance of rods of the salamander *ambystoma tigrinum*. *The Journal of Physiology*, 371(1):115–145, 1986.
25. EM Wells-Gray, SS Choi, A Bries, and N Doble. Variation in rod and cone density from the fovea to the mid-periphery in healthy human retinas using adaptive optics scanning laser ophthalmoscopy. *Eye*, 30(8):1135, 2016.
26. Michael L Hines and Nicholas T Carnevale. The neuron simulation environment. *Neural computation*, 9(6):1179–1209, 1997.
27. David Martin, Charless Fowlkes, Doron Tal, and Jitendra Malik. A database of human segmented natural images and its application to evaluating segmentation algorithms and measuring ecological statistics. In *Computer Vision, 2001. ICCV 2001. Proceedings. Eighth IEEE International Conference on*, volume 2, pages 416–423. IEEE, 2001.
28. Yunjin Chen and Thomas Pock. Trainable nonlinear reaction diffusion: A flexible framework for fast and effective image restoration. *IEEE transactions on pattern analysis and machine intelligence*, 39(6):1256–1272, 2017.
29. Martín Abadi, Paul Barham, Jianmin Chen, Zhifeng Chen, Andy Davis, Jeffrey Dean, Matthieu Devin, Sanjay Ghemawat, Geoffrey Irving, Michael Isard, et al. Tensorflow: A system for large-scale machine learning. In *OSDI*, volume 16, pages 265–283, 2016.

30. Fengyuan Zhu, Guangyong Chen, and Pheng-Ann Heng. From noise modeling to blind image denoising. In *Proceedings of the IEEE Conference on Computer Vision and Pattern Recognition*, pages 420–429, 2016.
31. Kostadin Dabov, Alessandro Foi, Vladimir Katkovnik, and Karen Egiazarian. Image denoising with block-matching and 3d filtering. In *Image Processing: Algorithms and Systems, Neural Networks, and Machine Learning*, volume 6064, page 606414. International Society for Optics and Photonics, 2006.
32. S Forti, A Menini, G Rispoli, and V Torre. Kinetics of phototransduction in retinal rods of the newt *triturus cristatus*. *The Journal of Physiology*, 419(1):265–295, 1989.
33. V Torre, S Forti, A Menini, and M Campani. Model of phototransduction in retinal rods. In *Cold Spring Harbor symposia on quantitative biology*, volume 55, pages 563–573. Cold Spring Harbor Laboratory Press, 1990.
34. Y Kamiyama, T O’Sura, and S Usui. Ionic current model of the vertebrate rod photoreceptor. *Vision research*, 36(24):4059–4068, 1996.
35. Steven Barnes and Bertil Hille. Ionic channels of the inner segment of tiger salamander cone photoreceptors. *The Journal of General Physiology*, 94(4):719–743, 1989.
36. Dmitri E Kourennyi, Xiao-dong Liu, Jason Hart, Farid Mahmud, William H Baldrige, and Steven Barnes. Reciprocal modulation of calcium dynamics at rod and cone photoreceptor synapses by nitric oxide. *Journal of neurophysiology*, 92(1):477–483, 2004.
37. Xiao-Dong Liu and Dmitri E Kourennyi. Effects of tetraethylammonium on kx channels and simulated light response in rod photoreceptorss. *Annals of biomedical engineering*, 32(10):1428–1442, 2004.
38. Rodrigo Publio, Rodrigo F Oliveira, and Antonio C Roque. A realistic model of rod photoreceptor for use in a retina network model. *Neurocomputing*, 69(10):1020–1024, 2006.